Acoustic Impedance Deblurring with a Deep Convolution Neural Network

Isaac Sacramento, Elton Trindade, Mauro Roisenberg, Fernando Bordignon, and Bruno Rodrigues

***Abstract*—Domain-specific methods for deblurring particular sorts of objects have gained increasing attention due to the ineffectiveness of generic methods. We present a simple and effective convolutional neural network that deblurs post-inversion acoustic impedance images. The architecture of our model consists of a convolutional layer that highlight edges and contours related to interfaces between rock layers; a locally-connected layer, that performs a convolutional step with unshared weights; finally, two fully-connected layers that perform a non-linear estimation of acoustic impedance values. We use the updated Standford VI reservoir model as training dataset, which is composed of 150 acoustic impedance sections, each section with 200 traces. In our work, we adopt a strong supervised learning that exploit, trace by trace, the dataset of the inverted and ground truth impedance images. We also present an analysis comparing the frequency bandwidth among the latent, blurry, and deblurred images. Furthermore, the peak signal-to-noise ratio (SNR) is calculated and compared with a classical deblurring method. We additionally address the requirement of deep learning for the huge amount of training examples by inserting rectified linear units (ReLU) and keeping the network architecture simple. The experimental results demonstrate the efficacy of the proposed method.**

***Index Terms*—convolutional neural network, acoustic impedance, deblurring, seismic inversion, frequency recovering.**

I. Introduction

THIS letter presents a deep convolutional approach for recovering high frequency components in post-inversion acoustic impedance models. Seismic acoustic impedance inversion is a process applied to seismic reflection data in order to infer rock density and compressional velocity, and thereafter other rock properties. eg.: porosity, lithology and net pay. When used to build an integrated model of the reservoir, seismic inversion provides several advantages: (1) it facilitates integrated interpretation, and (2) it optimizes the correlation between seismic and petrophysical properties of the reservoir, (3) if a stochastic method is used, it can improve data's vertical resolution.

Three different approaches for seismic inversion are mainly listed in literature: deterministic, stochastic, and geostatistical. Deterministic inversion is mainly useful for deriving general trends and highlighting large features in an exploratory stage. Despite the efficiency in terms of time consumption, in deterministic methods the vertical resolution remains constrained by the seismic bandwidth [3]. The results are obtained in terms of average solutions, thus generating blurry images. On the other hand, stochastic inversion uses random variation of parameters to reach results with vertical resolution that is superior to the conventional data. However, when working with multiple realizations, selecting the model that best characterizes the reservoir is difficult, since all of them are equally probable. Uniqueness problems are an issue mainly addressed by calculating the mean of different realizations. It has been proven that the mean solution is closer to a bandwidth limited solution, in such a way that the high frequencies features are lost [4]. Geostatistical methods perform similar to the stochastic ones, except by the addition of variogram models to ensure that the models fit expected spatial patterns.

The seismic vertical resolution is the minimal thickness that can be resolved by seismic. The most accepted value is a quarter of the wave length, that means that only layers thicker than that will be detected by seismic acquisition. In larger depths that value can be as high as 20 meters, which may represent a significant amount of oil volume being under or overestimated. Even though the inversion process can add low frequencies to the acoustic impedance spectrum through a constraint model, results from a typical post-stack or pre-stack seismic inversion are band-limited primarily due to missing the lowest and highest frequencies in the wavelet. Consequently, thin beds are generally poorly resolved [2].

An approach to deal with the high frequency impedance information out of the frequency bandwidth of seismic signal is assuming a blocked model for the earth's impedance [4]. This assumption is not always valid, and in some cases the high frequencies in the inverted impedance are ignored [5]. [6] aim to enhance the seismic acquisition resolution and, by consequence, achieving an improvement in seismic inversion and reservoir characterization, while [7] use wavelet frequency-dependent scaling to extend the amplitude spectrum of high and low-frequency axes in time domain. Instead, we first perform a deterministic inversion through *Maximum-a-Posteriori* (MAP) [21], [22], after, we apply a supervised machine learning approach as a post-inversion processing to recover the high frequency components not captured by the inversion method.

In this letter, we propose a new multichannel and multilayer Convolutional Neural Network (CNN) model to perform deblurring in post-inversion acoustic impedance. Each network layer maps higher level features originating in the previews

I. Sacramento and M. Roisenberg are with the Department of Computer Science, Informatics and Statistics Institute, Federal University of Santa Catarina, Florianópolis, Santa Catarina, Brazil (e-email: isaac.sacramento@posgrad.ufsc.br; mauro.roisenberg@ufsc.br).

E. Trindade is with Petrobras, Rio de Janeiro, Rio de Janeiro, Brazil (e-email: elton.trindade@petrobras.com.br).

F. Bordignon is with Cognitive and Connectionism Laboratory, Federal University of Santa Catarina, Florianópolis, Santa Catarina, Brazil (e-mail: f.bordignon@gmail.com).

B. Rodrigues is with Petrobras, Rio de Janeiro, Rio de Janeiro, Brazil (e-email: bbrodrigues@gmail.com).

layers through one-dimensional convolutional blur kernels. To perform this mapping, the kernels (also named weights) are adjusted by minimizing a loss function. The model enhances the resolution of acoustic impedance images trace by trace, resulting in sharper images with increased high-frequency bandwidth and lower noise. In order to train the model, we perform MAP inversion that commonly generates a band-limited acoustic impedance model. Then, the pairs of inverted blurry and latent images are normalized and presented to the network as input and target, respectively.

The core concept of our architecture is the combination of the convolutional, locally-connected and regression layers. Thus the convolutional layer learns the spatial structures existing in different acoustic impedance traces, the locally-connected layer individualizes and refines the resolution of these structures, finally, the regression layer performs the prediction of the property values. Thus, deblurring the acoustic impedance models, as a post-inversion refinement process, should lead to a more accurate interpretation of the impedance models.

The contributions of this work are threefold. First, according to our knowledge, it is the first to approach inversion resolution enhancement through a post-inversion refinement. Second, the proposed deep learning model effectively recovers the high frequency spectrum absent in the post-inversion acoustic impedance. Additionally, it corrects deformations existing in thin bodies caused by the inversion process. Third, our proposal shows to be more general than the state-of-art methods for inversion resolution improvement, since the CNN learns the high frequency based on different possible scenarios and freely solve the occurrences in the post-inversion images.

The remainder of this letter is organized as follows. Section II reviews the deblurring methods and the CNN, a popularly used deep learning technique. Section III describes the data used for training the CNN and the architecture of the proposed model. Section IV reports the experiments and results, and Section V concludes our work.

II. Theoretical Foundations and Related Works

Deblurring is generally modeled as the convolution of a blur kernel k with a latent image I:

$$y = k \otimes I + n \tag{1}$$

where n is the noise. Since k, I and n are unknown, the problem is highly ill-posed and admits infinite solutions for k and I. Blind deconvolution refers to the inference of the sharp image I, given only the blurry image y, without any knowledge regarding the kernel k and the noise n [8]. In contrast, if k is assumed to be known, the approach is called non-blind deconvolution [9]. Applying blind deconvolution generally implies in making assumptions on blur kernels and/or on latent images. For example, assuming sparsity of blur kernel or that natural images have super-Gaussian statistics. The second assumption leads to the use of image priors on inference process and, consequently, to the MAP estimation [10]. However, [11] show that deblurring methods based on this prior tend to favor blurry images over original latent images.

The Bayesian inference approach [11] outperforms the MAP based methods. It marginalizes the image from the optimization step, while estimating the unknown blur. According to [12], defining a gradient prior, by itself, is not sufficient to reach a sharp image, instead, they search in a dataset for a prior that densely correspond to the blurry image similar to a sharp image. Even though [13] suggest a generalization for the method proposed by [12], it still requires a similar reference image, which is not always available.

The methods described previously fail when applied to real world blurry images [14] and take a severe computational cost [15]. In contrast, the learning-based methods have gained attention with the resumption and recent advances in CNN. Currently, CNN is one of the most successful methods in computer vision. A basic architecture of a CNN model is composed of a convolutional layer with non-linear activation neurons, and a pooling layer. The convolutional layer takes into account a fixed-size and spatial location portion of the previous layer, and outputs a weighted representation of its input. Pooling layers calculate statistical summaries of spatial dimensions to down-sample feature maps. Thus, pooling layers can extract contextual information from a larger spatial context.

The adequate hyper-parameter adjustment allows a CNN learn non-linear function or blur kernels. Thus, deblurring becomes a function of a blurry image B and a set of parameters p as 2

$$y = \sigma(B, p) \tag{2}$$

Learning-based methods focus on developing a model to learn the function σ and to perform non-blind deblurring [15]. [16] teaches a CNN to recognize motion kernels and performs non-blind deconvolution in dense motion field estimate, in addition, [17] minimize regularized l_2 in order to perform text deblurring. In our approach, we perform a blind deconvolution by letting a CNN model to learn the unknown kernels that best deblur the acoustic impedance traces, based on the knowledge of the ground truth image and their correspondent seismic traces.

III. Data and Methods

A. Proposed Architecture

We propose a four-layer multichannel CNN architecture for deblurring post-inversion acoustic impedance images and recovering high frequency of thin layers. The model takes in each input channel the blurry acoustic impedance trace and the respective seismic profile. Additionally, by using the ground truth AI trace as target, the network is able to learn with the acoustic impedance data in association with the local seismic. The model consists of one convolutional layer and one locally-connected layer, each one of them followed by max pooling. The output of the locally-connected layer is flatted and two fully connected layers are added in the end (Fig. 1).

The first convolutional layer deblurs the lower features in the input traces. Following, higher features are individually deblurred through a locally-connected layer, which performs a one-dimensional convolution with unshared weights. Thus, instead of performing standard convolution, the weights of the learned kernel matrices are not shared across the input.

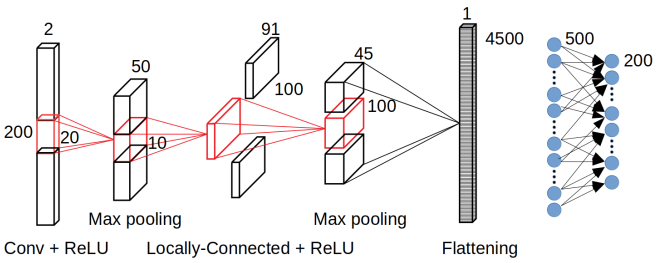

Fig. 1. Proposed architecture for trace-by-trace deblurring of post-inversion acoustic impedance images.

The number of filters in the convolution and locally-connected layers is 50 and 100, respectively. As the number of filters increases from the first to the second layer, the size of each filter decreases from 20 to 10. This way, we note that the CNN learns thinner geological bodies in the second layer.

We use rectified linear unit (ReLU) function that is one of the most popular and efficient activation functions for CNNs. There are advantages of using ReLU such as efficient computation, and gradient propagation. The network uses Adam to optimize the loss function. This algorithm combines the AdaGrad and RMSProp methods and converges more efficiently in comparison to gradient descent, stochastic gradient descent, AdaGrad and RMSProp [18]. The Mean Absolute Error (MAE) is the loss function minimized in the training process.

B. Dataset

To evaluate the proposed deblurring method, an acoustic impedance data set is collected[1]. The dataset contains a cube of acoustic impedance values from the updated Stanford VI reservoir [19], which is represented by a three-dimensional regular stratigraphic model. The cube contains 150x200x200 cells and the dimensions of each cell are 25 meters horizontally and 1 meter vertically. The model represents a fluvial channel system composed of three layers: the deepest one represents deltaic deposits (layer 3), the middle layer represents meandering channels (layer 2) and the shallowest layer (layer 1) sinuous channels, deposited in the fluvial channel system [2]. Some sample images from Stanford VI are shown in Fig. 2 Even though the data has been synthetically generated, the layers represent geological bodies of high importance in reservoir characterization, such as channels connections and theirs discontinuity.

In a realistic scenario, the number of hard data available for training and validating supervised models is scarce. In order to address this common issue, we performed experiments with constrained amount of training data, set to 50%, 33% and 10% of the available data. Using 50% and 33% produces similar results in the frequency spectrum, whereas 10% showed more significant discrepancies in the amplitude recovering and additional noise mainly in higher frequencies (Fig. 3). Therefore, in the following experiments we adopted 30% of available data as training data set, once we observed it is the minimum amount of data to keep the model learning capability.

[1]Available at https://github.com/SCRFpublic/Stanford-VI-E/tree/master/Acoustic%20Impedance

[2]See [20] for more details about methodologies and model parameters.

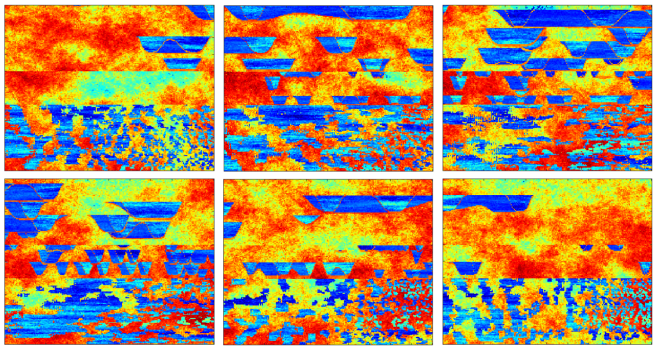

Fig. 2. Sample images from the updated Standford VI data set used in this letter. The images dimensions are 200 traces, each one with 200 cells along the depth.

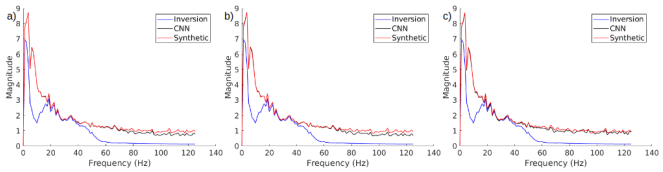

Fig. 3. Frequency magnitude graphs for ground truth, inverted acoustic impedance, and deblurred acoustic impedance. (a) Using 50% of the total data set as training data. (b) Using 33% of the total data set as training data. (c) Using 10% of the total data set as training data. In (c) is observable additional peaks of noisy high-frequency between the peaks of the ground truth image.

To build the training data set we carry out the *Maximum-a-Posteriori* (MAP) [21], [22] inversion at the seismic data generated by the high resolution acoustic impedance, which is our ground truth. In order to proceed the inversion, we created a Ricker wavelet with frequency bandwidth from $0Hz$ to $60Hz$, with which the synthetic seismic was calculated through the forward model. Additionally, a low frequency model was calculated by applying a low-pass filter with $4Hz$ cutting frequency to the original acoustic impedance . Thus, the *a posteriori* acoustic impedance cube was calculated and the pair of truth and inverted images compose the training data set. As expected, the inverted acoustic impedance bandwidth is restricted to the wavelet bandwidth with addition of the spectrum of the low frequency model. Due to the 1D convolution adopted in this work, the training data set contains 10000 trace samples with 200 cells along the depth. Each group of 200 traces composes a section of the cube.

IV. Experiment and Discussion

Here, we validate the proposed post-inversion deblurring method. The parameters settings for the model training are presented. Next, the experimental results are given for the proposed method, as well as the comparison methods.

A. Model Training

We will use 33% (10000 traces) of the available data, seismic and inverted acoustic impedance traces, to infer the

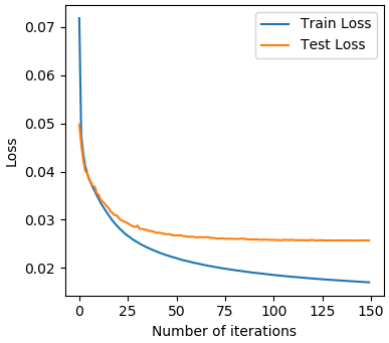

Fig. 4. Training and testing losses of CNN.

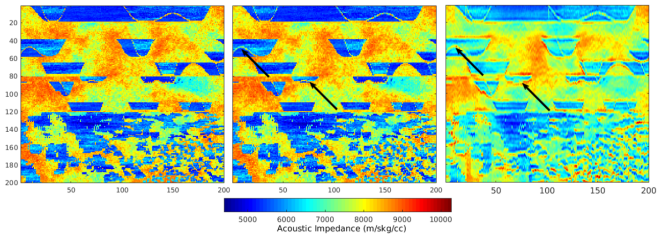

Fig. 5. Visual close-ups of CNN deblur results on test set. Thin bodies and layer intersections are highlighted. From left to right: ground truth, CNN result and MAP result.

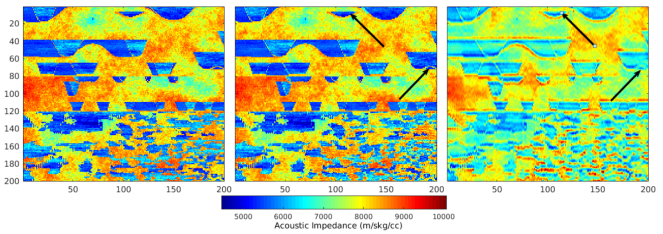

Fig. 6. Visual close-ups of CNN deblur results on test set. Deformed bodies are precisely recovered and vertical resolution is improved. From left to right: ground truth, CNN result and MAP result.

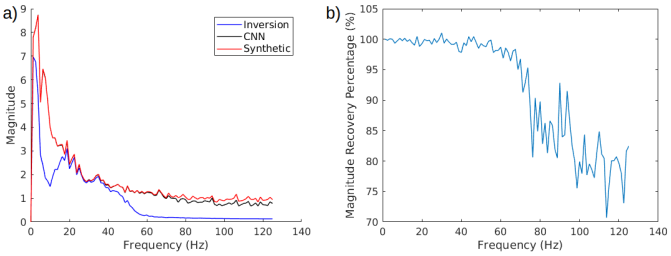

Fig. 7. Frequency spectrum comparison between the ground truth image, the MAP inversion image and the deblurred image. Additionally, the recovery percentage for each frequency magnitude is introduced.

blur filters. Furthermore, we will adopt mini-batches with size of 10 training examples and exponentially decreasing learning rate (initially set to 0.001) in a total of 150 iterations.

The network contains two channels in the input layer and we set each input data with one channel. We deal with this issue of over-fitting by calculating the loss for the test images, and controlling the training, thus we early stop the training as soon as the test loss stops decreasing (Fig. 4). Other techniques to avoid over-fitting, such as drotout, compromised the reconstruction of the entire image. The network weights initialize randomly and the model perform supervised learning over tuples containing the pairs of inverted acoustic impedance and seismic profile as input, and ground truth traces as targets. To avoid neuron saturation and still keep the non-linearity predictability of the CNN, we normalize the acoustic impedance to values between 0 and 1.

B. Deblurring Post-Inversion Acoustic Impedance

By applying the trained model to a set of inverted traces, we notice that the CNN produced overall shaper acoustic impedance images. Looking into the details, the deblurred images show substantial recovery of high frequency events (thin layers), which can be seen in the intersections between two channels, as illustrated in Fig. 5.

It should be pointed out that the horizontal resolution seem to be better enhanced when compared to the vertical resolution, which can be an effect of the wavelet signature and/or the de-convolution process. The increase in the horizontal resolution is particularly important, since it is related to events in which the layers become thinner and the porosity decreases, thus decreases the impedance contrast and, therefore, its seismic response. The vertical resolution improvement is essential to evaluate the vertical connectivity in the reservoir. In terms, it is possible that thin layers of shale act as barriers for the water injection and affect the production and pressurization of the reservoir. Besides significant improvements in the resolution, the model managed to correct some geometric deformations created during the inversion process (Fig. 6), which usually occurs in smaller depositional features, as channels.

A relevant aspect in deblurring acoustic impedance images is the observance of high frequencies recovering after the blurry images being submitted to the CNN. Moreover, the additional spectrum is associated to the insertion of high frequency signal, instead of noise. Fig. 7 introduces the graphs containing the frequency magnitudes of our test examples, as well as the recovery percentage for each frequency magnitude. As can be noticed, the CNN recovered around 100% of the signal frequency existing in the blurry image (from $4Hz$ to $60Hz$). The model recovered the total frequency in the spectrum lower than $4Hz$, as long as from 70 to 90% of the possible frequencies in the spectrum higher than $60Hz$. Since these ranges of frequencies are absent in the inverted acoustic impedance, we note that the CNN learned the existing relation between the seismic profiles and the acoustic impedance in the ground truth images and correctly rebuilt them in the test images.

In addition, we calculated the peak signal-to-noise ratio (PSNR) of each test section. Tab. I list the values of PSNR for the ground truth image, for the inversion result, and the image deblurred with the classical method using wiener filters, and our proposal. The proposed method holds clearly higher performance than the classical method, since it generates image with higher PSNR. This result endorses that the high frequency components recovered by the CNN is related to

TABLE I
RESULTS EVALUATED ON UPDATED STANDFORD VI RESERVOIR, EXAMPLES INTRODUCED IN FIG. 5 AND FIG. 6. PSNR (DB) IS LISTED.

Image Section	*Inversion (dB)*	*Wiener Filter (dB)*	*Our (dB)*
Fig. 5	19.7249	26.0915	27.9108
Fig. 6	19.5143	26.2077	27.4851

signal, rather than noise.

V. CONCLUSION

In summary, we proposed a multichannel and multilayer CNN for post-inversion acoustic impedance deblurring. Moreover, we introduced a simple architecture that combines convolution, locally connected and regression layers. We demonstrated that the CNN achieved reasonable results regarding the high frequency recovering in seismic inversion data. The methodology is promising for deblurring post-inversion acoustic impedance due to its capability to learn one-dimensional blur kernels and to recover two-dimensional geometric features (such as deposition borders and thin layers). We tested the model on a synthetic data set, with limited amount of example images, and significantly realistic in its structure and dimensions. In order to go further in realistic and comprehensive training data, the model may be fed with shallower portions of the seismic data. This approach is feasible, since most geological features tend to repeat themselves (fractal theory) where the frequency spectrum is broader in the high frequencies, i.e, the frequency amplitude decreases exponentially with depth, due to attenuation and dispersion effects during propagation.

ACKNOWLEDGMENT

The authors would like to thank *Conselho Nacional de Pesquisa e Desenvolvimento, Fundação de Amparo à Pesquisa e Inovação do Estado de Santa Catarina* and Petrobras for their support and availability during the work.

REFERENCES

[1] S. S. Sancevero, A. Z. Remacre, R. S. Portugal, "O papel da inversão para a impedância no processo de caracterização sísmica de reservatórios", in Revista Brasileira de Geofísica, p. 495–512, v. 24, 2006.

[2] R. Zhang and M. K. Sen and S. Phan and S. Srinivasan, "Stochastic and deterministic seismic inversion methods for thin-bed resolution", Journal of Geophysics and Engineering, V. 9, N. 5, 2012.

[3] S. S. Sancevero and A. Z. Remacre and R. de S. Portugal and E. C. Mundim, "Comparing deterministic and stochastic seismic inversion for thin-bed reservoir characterization in a turbidite synthetic reference model of Campos Basin, Brazil", The Leading Edge, v. 24, num. 11, pp. 1168–1172, 2005.

[4] D. Cooke and J. Cant and A. Santos and P. Wa, Australia, "Model-based Seismic Inversion: Comparing deterministic and Probabilistic approaches". CSEG Recorder, 2010.

[5] S. Yuan and S. Wang and C. Luo and Y. He, "Simultaneous multitrace impedance inversion with transform-domain sparsity promotion", Geophysics, pp. 71–80, v. 80, n. 2, 2015.

[6] X. Xiaoyu, L. Yun, S. Desheng, G. Xiangyu, and W. Huifeng, "Studying the effect of expanding low or high frequency on post-stack seismic inversion", in SEG Technical Program Expanded Abstracts 2012, pp. 1–5, 2012.

[7] S. Chen and Y. Wang, "Seismic Resolution Enhancement by Frequency-Dependent Wavelet Scaling", in IEEE Geoscience and Remote Sensing Letters, no. 99, pp. 1–5, 2018.

[8] H. Zhang, D. Wipf and Y. Zhang, "Multi-image Blind Deblurring Using a Coupled Adaptive Sparse Prior", IEEE Conference on Computer Vision and Pattern Recognition, Portland, OR, pp. 1051–1058, 2013.

[9] C. Wang, L. Sun, Z. Chen, S. Yang and J. Zhang, "High-quality non-blind motion deblurring", 16th IEEE International Conference on Image Processing (ICIP), Cairo, pp. 153–156, 2009.

[10] S. D. Babacan, R. Molina, M. N. Do, and A. K. Katsaggelos, "Bayesian blind deconvolution with general sparse image priors", in Proceedings of European Conference on Computer Vision (ECCV), pp. 341–355, 2012.

[11] A. Levin, Y. Weiss, F. Durand, and W. T. Freeman. "Understanding and evaluating blind deconvolution algorithms", In IEEE Proceedings of International Conference on Computer Vision and Pattern Recognition (CVPR), pp. 1964–1971, 2009.

[12] Y. Hacohen, E. Shechtman, and D. Lischinski, "Deblurring by example using dense correspondence", In IEEE Proceedings of International Conference on Computer Vision (ICCV), pp. 2384–2391, 2013.

[13] J. Pan, Z. Hu, Z. Su, and M. H. Yang, "Deblurring face images with exemplars", In Proceedings of European Conference on Computer Vision (ECCV), pp. 47–62. Springer, 2014.

[14] W.S. Lai, J. B. Huang, Z. Hu, N. Ahuja, and M. H. Yang, "A comparative study for single image blind deblurring", In IEEE Proceedings of International Conference on Computer Vision and Pattern Recognition (CVPR). IEEE, 2016.

[15] A. Chakrabarti, "A neural approach to blind motion deblurring", In Proceedings of European Conference on Computer Vision (ECCV), pp. 221–235, Springer, 2016.

[16] J. Sun, W. Cao, Z. Xu, and J. Ponce, "Learning a convolutional neural network for non-uniform motion blur removal", In IEEE Proceedings of International Conference on Computer Vision and Pattern Recognition (CVPR), pp. 769–777, 2015.

[17] M. Hradis, J. Kotera, P. Zemcık, and F. Sroubek, "Convolutional neural networks for direct text deblurring", In Proceedings of British Machine Vision Conference (BMVC), 2015.

[18] D. P. Kingma and J. Ba. "Adam: A method for stochastic optimization", Unpublished paper. [Online]. Available: https://arxiv.org/abs/1412.6980, 2014.

[19] Lee, J. and Mukerji, T., "The Stanford VI-E reservoir: A synthetic data set for joint seismic-EM time-lapse monitoring algorithms", 25th Annual Report, Stanford Center for Reservoir Forecasting, Stanford University, Stanford, CA, 2012.

[20] Castro, S., Caers, J., and Mukerji, T., "The Stanford VI reservoir": 18th Annual Report, Stanford Center for Reservoir Forecasting, Stanford University, Stanford, CA, 2005.

[21] A. Buland, and H. Omre, "Bayesian linearized avo inversion", In Geophysics, pp. 185–198, 2003.

[22] L. P. Figueiredo, M. Santos, M. Roisenberg, G. Neto, and W. Figueiredo, "Bayesian framework to wavelet estimation and linearized acoustic inversion", in Geoscience and Remote Sensing Letters, pp. 1–5, 2012.